Bedding surface roughness profiles and estimated dilation angles

Dwayne Tannant
School of Engineering – University of British Columbia - Okanagan, Kelowna, BC, Canada
Navid Bahrani
Department of Civil & Environmental Engineering – University of Alberta, Edmonton, Alberta, Canada
Vikram A. Gulati
Department of Mining Engineering, IIT Kharagpur, India

ABSTRACT

Methods suggested to measure rock surface roughness have been mostly applied to small artificial or laboratory specimens. Results are presented from different methods to calculate the roughness using a detailed field-scale digital terrain model developed using photogrammetry techniques. Profiles of a bedding surface that was involved in a large slab failure were generated from the digital terrain model. These profiles were used to assess the dilational component of the shear strength for the bedding surface.

RÉSUMÉ

Des méthodes suggérées pour mesurer la rugosité extérieure de roche ont été la plupart du temps appliquées à de petits spécimens artificiels ou de laboratoire. Des résultats sont présentés de différentes méthodes pour calculer la rugosité en utilisant un modèle numérique de plein champ détaillé de terrain développé en utilisant des techniques de photogrammétrie. Des profils d'une surface de literie qui a été impliquée dans un grand échec de galette ont été produits du modèle numérique de terrain. Ces profils ont été employés pour évaluer le composant de dilational de la résistance au cisaillement pour la surface de literie.

1 INTRODUCTION

The topology or roughness of steeply dipping bedding planes has an influence on the shear strength of these structures and hence on the slope stability of footwall slopes constructed in mountainous coal mines in western Canada. Typically slope designs are based on simple limit equilibrium approaches and estimates of shear strength expressed in terms of cohesion and friction angle. For friction angle, most practitioners use a conservative base or residual angle of friction. However, the roughness present on the sliding surface increases the shear strength and when designing steep mining slopes an assessment of this roughness or dilational component is useful.

Most published work on characterizing rock surface roughness has been done on laboratory scale specimens. This paper applies characterization techniques to much larger field scales. Roughness profiles at field scales can be measured using laser scanners or photogrammetry-based digital terrain models. This approach was adopted to characterize a steeply dipping bedding surface associated with a footwall slope that failed at a western Canadian coal mine in 2006 (Tannant & LeBreton 2007). The failure likely involved planar slab sliding combined with buckling and/or toe shear. The failure occurred in two stages separated by two weeks and ultimately involved a surface area of approximately 11140 m^2 with an average slab thickness of 5.4 m giving a failed volume of approximately 60,000 m^3. Assuming the rock density was 2500 kg/m^3 yields a failed mass of 150,000 tonnes. Further details on the geology and failure conditions can be found in Tannant and LeBreton (2007).

A photogrammetry survey of the 60 m high footwall slope was conducted two weeks after its failure. Stereo photographs (Figure 1) obtained from the survey were processed to generate a digital terrain model (DTM) using Adam Technologies CalibCam and Analyst software (Birch 2006). The digital terrain model of the exposed bedding surface upon which the slab failure had occurred had 427160 points and 854302 triangles. The area of the model was 5233 m^2, thus the average point density of the digital terrain model of the sliding surface was calculated to be 81.6 points/m^2.

2 BEDDING SURFACE PROFILES

Seven north-south vertical 2D profiles were taken through the DTM. These were used to measure the variation of roughness along the sliding surface in the direction of sliding. The vertical cross-sections were taken at 10 m intervals of Easting across the slope (Figure 2). The average length of the profiles was

25 m. The distance between coordinates along each profile varied between 2 and 120 mm with an average of about 20 mm. The 2D profiles were used to measure various surface roughness parameters and ultimately assess the dilational component of the shear strength for the bedding surface involved in the slab failure.

Figure 1. Image of the footwall slope after slab failure

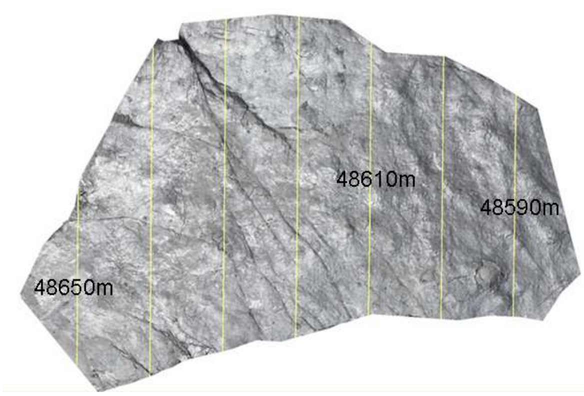

Figure 2. Vertical cross sections on the bedding surface at different Eastings

It is assumed that the roughness of the measured post-failure profiles is the same as that present before the slab failure occurred. Hence, the dilational component of the shear strength could be assessed from the post-failure roughness of the slip surface. The estimated residual friction angle for the bedding surface is 22º to 25º based on past experience in western Canadian coal mines.

The profiles extracted from the DTM were first plotted in a spreadsheet and a linear regression line was drawn through all the points of each profile. The regression analysis was done to check the overall linearity of the profile. Since long profiles were obtained from the DTM model, portions of a profile may deviate from an overall near-planar shape and can be termed as non stationary. Characterizing the roughness of non-planar profiles can lead to inaccurate results. All the profiles had linear regression coefficients (R-squared values) greater than 0.9. The data density was sufficient to satisfy the requirement for calculating the roughness parameters. Figure 3 shows two typical bedding surface profiles. Both profiles appear to be fairly planar at this scale.

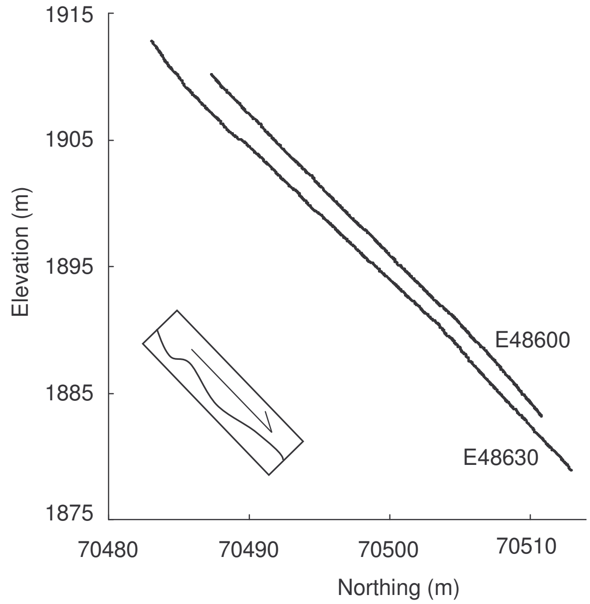

Figure 3. Post failure profiles used to measure failure surface roughness and dilation angle

Once linear sections of the profiles were selected they were rotated to create horizontal profiles. Figure 4a and Figure 4b shows the smoothest and roughest profile, respectively. The transformed profiles were used for calculating the roughness parameters for each profile. The joint roughness coefficient, *JRC*, and dilation angle, *i* are useful because they can be directly related to the shear strength of the bedding surface.

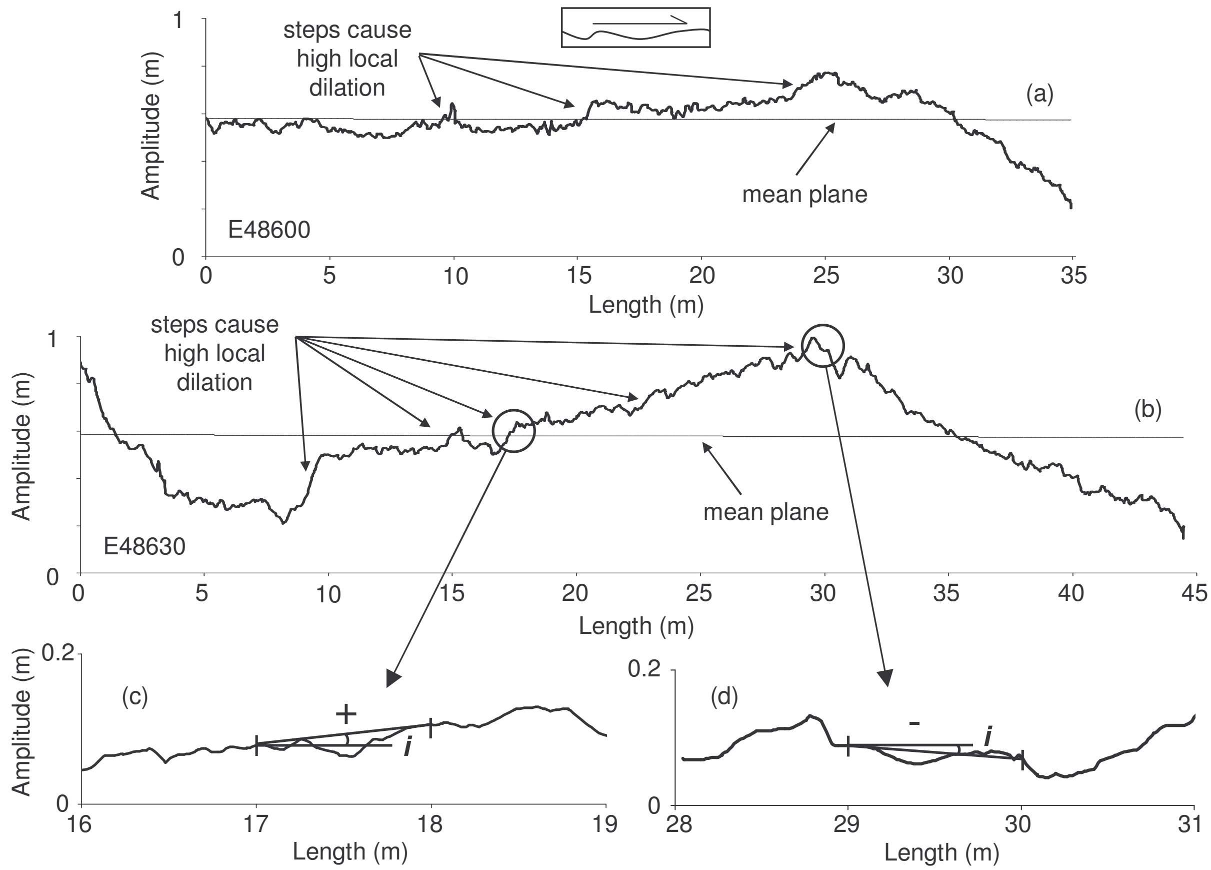

Figure 4. Two typical profiles transformed to the horizontal axis with exaggerated vertical scale

3 ROUGHNESS CHARACTERIZATION

3.1 Joint roughness coefficient

The roughness of a rock surface affects the shear strength of that surface. A commonly used method to incorporate roughness within an expression of shear strength is to use the joint roughness coefficient, *JRC* in Barton's (1973) empirical equation:

$$\tau = \sigma_n \tan\left(\phi + JRC \log\left(\frac{JCS}{\sigma_n}\right)\right) \quad [1]$$

where σ_n is the effective normal stress and *JCS* is the joint wall compressive strength. *JCS* is often taken as the rock uniaxial compressive strength for a fresh joint sample (Bandis et al. 1983) and the ratio JCS/σ_n is restricted to values less than 100. In this equation, the effective dilation angle *i* as defined by Barton and Choubey (1977), is given by:

$$i = JRC \log\left(\frac{JCS}{\sigma_n}\right) \quad [2]$$

The *JRC* values typically vary between 0 and 20, and are usually obtained by comparing the appearance of laboratory-scale joint profiles with the typical roughness profiles published by Barton (1973) and Barton and Choubey (1977).

It is likely that *JRC* values decrease with increasing scale. Barton and Bandis (1980) suggested that longer profiles have lower *JRC*. Barton and Bandis (1990) used a scale correction for *JRC* using:

$$JRC_n = JRC_o \left(\frac{L_n}{L_o}\right)^{-0.02\, JRC_o} \quad [3]$$

where: JRC_o, and L_o (profile length) refer to 100 mm laboratory scale samples while L_n and JRC_n refer to *in situ* block size and field scale joint roughness coefficient. If *JRC* is measured or estimated from a laboratory specimen or rock core, then this value can be adjusted downward as a method to estimate the effective roughness at the field scale.

According to the results of laboratory direct shear tests (100 mm size) reported by Dawson (1990) the average coal JRC_o is 3.5. Simply assuming a range in field scale from 1 to 10 m yields adjusted *JRC* values that are listed in Table 1.

Table 1. *JRC* for profiles 48600 and 48630

profile	Base length 1 m	2.5 m	5 m	10 m
All[1]	2.98	2.79	2.66	2.54
48600[2]	5 to >20	5 to 20	5 to 12	8
48630[2]	5 to >20	5 to >20	6 to 20	6 to 16

[1, 2] refer to the 1st and 2nd method

Barton and Bandis (1990) described a second method for estimating the field scale *JRC*. This method was also reviewed by and Hoek (2007) and is shown in Figure 5. The approximate JRC_n values can be determined from the measured values of the amplitudes and lengths of joint profiles.

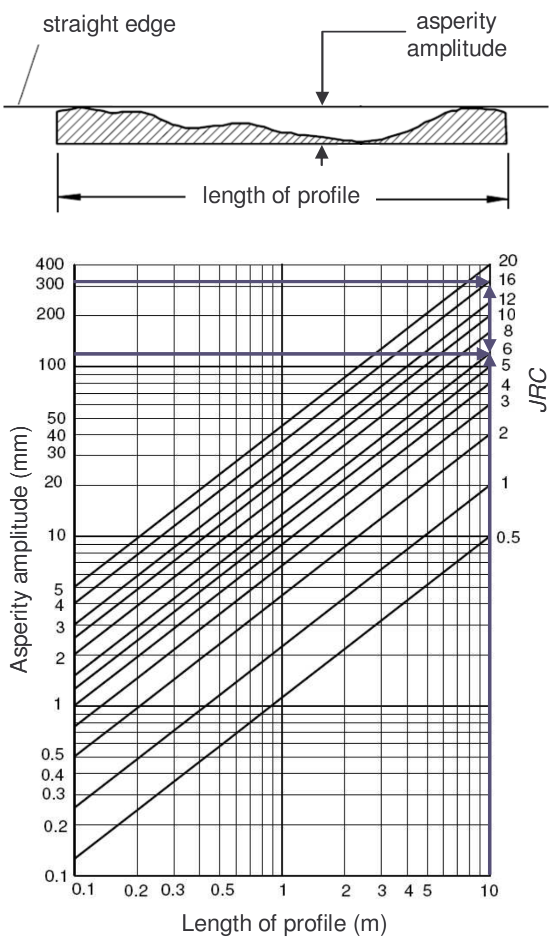

Figure 5. *JRC* field estimation of profile E48630 for a base distance of 10 m (after Barton and Bandis 1990)

Each profile was divided into a sequence of segments using set base distances of 1, 2.5, 5 and 10 m. The best-fit line through each segment was again obtained and transformed to the horizontal axis. The amplitude of the profile was used with Figure 5 to estimate the field-scale *JRC*. The values are listed in Table 1. Clearly these values are much higher than those estimated by merely scaling limited laboratory shear testing data. It is highly unlikely that the effective *JRC* for the bedding planes is larger than 10. This casts doubt on the reliability of the method based on Figure 5 for estimating *JRC* at the field scale.

The third technique used here for estimating the joint roughness coefficient from profile data is based on the equations given by Yang et al. (2001):

$$JRC = 32.69 + 32.98 \log_{10} Z_2 \qquad [4]$$

$$Z_2 = \left[\frac{1}{M(\Delta x)^2} \sum_{i=1}^{M} (y_{i+1} - y_i)^2 \right]^{1/2} \qquad [5]$$

where Z_2 is the root mean square of the tangents of the slope angles along the profile, Δx is the constant distance lag, M is the number of intervals and y is the height of the profile.

To estimate the *JRC* using these equations, some of the original profiles were trimmed to a shorter length to make them appear more linear and thus reduce the non stationary aspect of these profiles. This is very important for accuracy as the non stationary profiles give inaccurate results (Kulatilake et al., 2006; Yang et al., 2001, Kulatilake and Um 1999; Kulatilake et al., 1997). These profiles were then resampled at constant lag distance Δx before calculating the *JRC*.

The sampling ratio $\Delta x/L$ = 1/200 was kept the same as that used by Tse and Cruden (1979) and Yang et al. (2001) in formulating the *JRC* estimation. The *JRC* values obtained for the vertical profiles are shown in Table 2.

Table 2. *JRC* values for vertical profiles

Easting (m)	Trimmed profile length (m)	Lag distance (m)	*JRC*
48650	22.3	0.11	3.9
48640	44.9	0.23	2.9
48630	45.2	0.23	1.4
48620	43.8	0.22	1.4
48610	37.2	0.17	0.8
48600	35.8	0.18	na
48590	30.3	0.15	1.0

The *JRC* varies in the range of 1 to 4. These fairly low values seem consistent with the geological history associated with the local folding and shearing and thrust faults in the area. Shear and slip would have occurred in the dip direction to accommodate the folding, thus probably contributing to a low roughness observed for the bedding surface as seen in Figure 1 and as measured along the vertical profiles.

The values of *JRC* at the field scale determined using the third method (Table 2) are believed to be much more reliable than the first two methods presented in this paper, especially those found using Figure 5.

3.2 Dilation angle

The dilation angles for two profiles were estimated based on the work introduced by Rengers (1970) and Schneider (1976) and described by Goodman (1989). First, each profile was resampled at a constant spacing of 0.5 m. Then the slope connecting sequential pairs of points that were spaced at base distances of 1, 2.5, 5, 10, and 20 m were calculated. A series of inclination angles at each base distance were obtained.

Figure 4c and Figure 4d show two inclination angles for two different parts of profile E48600 that were obtained based on a base distance of 1 m. As can be seen, some inclination angles are negative. As indicated by Grasselli et al. (2002), asperity surfaces that face the direction of shear will deform and cause dilation. Conversely, asperity surfaces inclined with the shear direction unload and open up and have no influence on dilation. Therefore, since the slab slid from left to right as shown on this figure and the asperities facing the shear direction have positive inclination angles, only inclination angles with positive values were collected and used in the analyses.

The inclination angles were plotted against their corresponding base distance, and an envelope through the maximum angles was drawn as shown in Figure 6a and Figure 7a. A series of secants associated with the maximum inclination angles for each base distance was drawn (Figure 6b and Figure 7b). The dilation curve was then developed by drawing the best fit line through all the points described by the maximum inclination angle for each base distance (Figure 6b and Figure 7b). Both dilation curves have regression coefficients (R-squared values) greater than 0.9.

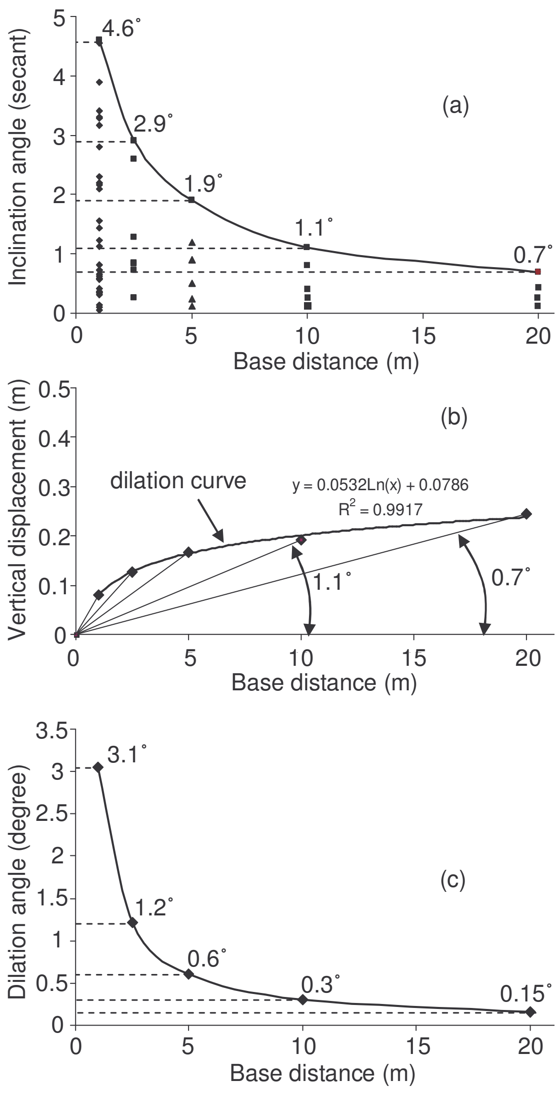

Figure 6. (a) Envelope through the maximum inclination angles (b) dilation curve and (c) dilation angle for different base distances for profile E48600

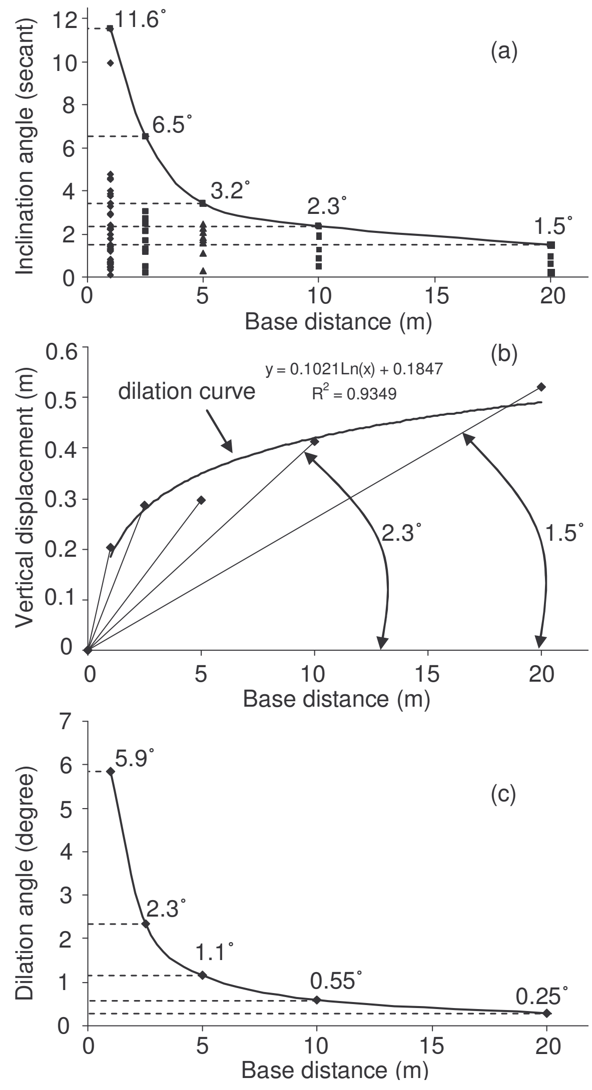

Figure 7. (a) Envelope through the maximum inclination angles (b) dilation curve and (c) dilation angle for different base distances for profile E48630

The dilation angles were then determined by measuring the slope of the tangent to the dilation curves for a given base distance (differentiating the dilation curve equations) as shown in Figure 6c and Figure 7c. The dilation angles decrease as the base distance increases from 1 to 20 m. This figure also shows that there is no single dilation angle for a profile. Moreover, this angle differs at different locations on the sliding surface and varies with changing the base distance.

It is difficult to determine what dimension is most appropriate for estimating the effective dilation angle that existed along the sliding surface. The larger pieces of slabs seen in the rubble pile at the base of the slope (Figure 1) had dimensions between 5 and 10 m. Using these dimensions to estimate the effective range of dilation angles yield values between 0.3º and 1.1º. The dilation angle lies between 3º and 6º when the base distance is reduced to only 1 m.

The field scale values of *JRC* can be converted into dilation angles using Equation 2. The conversion process requires an estimate of the effective normal stress and the strength of the asperities along the bedding surface. For the footwall, the sliding surface was mudstone or siltstone with a thin intermittent carbonaceous layer or thin (<80 mm), high ash coal seam. The mudstone or siltstone rock base of the sliding surface had undulations that formed larger scale asperities that are seen in the profiles. These rock asperities have an estimated unconfined compressive strength between 10 and 50 MPa. The normal stress was estimated to about 0.1 MPa for a slab 5.4 m thick dipping at about 50º. Thus the ratio JCS/σ_n ranges from 100 to 500 but will be limited to a value of 100 as per the recommendation by Barton (1973). Using Equation 2, the dilation angles calculated using the *JRC* values listed in Table 2 ranged from 2° to 8°.

Assuming that the approach adopted to determine field scale *JRC* values in Table 2 is correct and that the Barton (1973) relationship between *JRC* and dilation angle is valid, then comparison of dilation angles with the approach used in Figure 6 and Figure 7 suggests that the appropriate base distance is somewhere between 1 and 5 m.

4 IMPLICATIONS FOR BEDDING SURFACE SHEAR STRENGTH

The linear Mohr-Coulomb failure criterion is commonly used for limit equilibrium analysis of various failure mechanisms associated with steep footwall slopes. The base or ultimate friction angles for carbonaceous bedding planes are estimated to range from 22º to 25º (Hebil 2006). Thus if the dilation angle of the sliding surface was about 2º to 8º, then dilation could contribute about 10% to 25% of the peak effective frictional strength.

Based on a simple back-analysis of planar sliding, the estimated Mohr-Coulomb shear strength parameters for shearing along coal bedding surfaces at this location are cohesion of 30 to 50 kPa and peak friction angle of 23° to 25° (Tannant & LeBreton 2007). In this analysis, any potential contribution to shear strength from dilation was embedded in the cohesion term. Thus the back-calculated cohesion of 30 to 50 kPa, which is a significant component of the bedding surface shear strength, implicitly includes some dilation.

The Barton (1973) shear strength criterion (Equation 1) does not include cohesion because it was developed for non-bonded joint surfaces. One can estimate Mohr-Coulomb strength parameters using Equation 1. Assuming JCS/σ_n is about 100, *JRC* is 1 to 4, base friction angle is 22º to 25º, and fixing a tangent line to Equation 1 at 0.1 MPa normal stress yields Mohr-Coulomb shear strength parameters of c = 0 to 4 kPa and ϕ = 24º to 31º. Thus using the Barton (1973) approach would suggest using cohesion of essentially zero along with an effective peak friction angle of 24º to 31º.

In reality there was probably considerable cohesive strength present along the bedding surface before mining began arising from mineral bonding and other diagenesis processes. As mining progresses, the cohesive component of the shear strength diminishes because of shear displacements and shear stress reversals imposed upon the bedding surface as the open pit floor was mined past the slab location (Bahrani & Tannant 2008) and due to stress relief and blasting disturbances. These disturbances progressively rupture mineral bonds. How much true cohesion remains along the bedding surface once mining fully exposes the slab is unknown. It is prudent and conservative to assume that the cohesion drops to zero when designing steep footwalls while also recognizing that footwall slopes much steeper than the peak angle of friction can remain standing for a period of time.

For the sake of comparison, a series of horizontal profiles were taken from the DTM and values of *JRC* and dilation angle were calculated using the Yang et al. (2001) and Rengers (1970) methods. These profiles were ‘rougher’ and yielded slightly larger *JRC* values and dilation angles. This was expected given the nature of the folding and resulting flexural slip that probably occurred predominantly in the dip direction of the bedding surface and not along the strike direction.

It is very likely that the overall slab broke into many smaller pieces at onset of the failure. This was probably triggered by non-planarity of the bedding surface at the scales of 1 to 10 m as seen in Figure 4. The large-scale asperities or inflection points along the slope caused localized high dilation and bending during the initial sliding stages. The dilation angle calculated for base distances of 1 to 10 m varies between 0.3º and 3º for profile 48600 and 0.6º and 6º for profile 48630. While these are not large angles they were probably sufficient to cause tensile fracturing of the sliding slab into numerous smaller slabs. Interestingly, the subsequent stability of these smaller slabs may be governed by higher frictional strength (larger dilation angles) but lower or zero cohesive strength compared to the original bench-scale slab.

CONCLUSIONS

A detailed digital terrain model derived from terrestrial photogrammetry was used to generate profiles along a steep footwall slope at a coal mine that had experienced a multi-stage slab failure. The bedding surface profiles were used to characterize the geometric roughness in the sliding direction in order to estimate the contribution of the roughness to the bedding surface shear strength.

The field-scale *JRC* was estimated with three different techniques. Interestingly, a technique suggested by Barton and Bandis (1990) and found in Hoek's Notes (Hoek 2007) gave very high and unrealistic values for field-scale *JRC* values. A technique originally proposed by Tse and Cruden (1979) gave reasonable results. Another simple geometric technique (Goodman 1989) that directly calculates the maximum dilation angle for varying base distances yielded results that seem fairly reliable.

For the bedding surface, the estimated effective dilation angle was in the range of 2º to 8º. Given that the base or residual friction angle for carbonaceous bedding planes is only about 22º to 25º, the additional dilational component of the shear strength can be significant.

The ability to quickly and safely acquire detailed digital terrain models using photogrammetry or LiDAR techniques improves our ability to characterize the shear strength of steep footwall slopes. Better estimation of the peak or effective friction angles present in a slope opens up opportunities to better constrain the more elusive cohesive component of shear strength.

ACKNOWLEDGEMENTS

Grande Cache Coal Ltd. kindly provided access to the open pit containing the steep bedding surface numerous times over a two-year period and provided survey data required to georeference and scale the digital terrain models.

REFERENCES

Bahrani N. & Tannant D.D. 2008. Shear strength assessment of a footwall slab using finite element modelling. *Canadian Institute of Mining and Metallurgy Conference & Exhibition,* Edmonton.

Bandis S.C., Lumsden A.C. & Barton N. 1983. Fundamentals of rock joint deformation. *Int. J. of Rock Mech. and Min. Sci.*, **20**: 249-268.

Barton N.R. 1973. A review of a new shear strength criterion for rock joints. *Engineering Geology*, **7**: 287-322.

Barton N. & Choubey V. 1977. The shear strength of rock joints in theory and practice. *Rock Mechanics*, **10**: 1-54.

Barton N. & Bandis S.C. 1980. Some effects of scale on the shear strength of joints. *Int. J. of Rock Mechanics and Mining Sci.,* **17**: 69-73.

Barton N. & Bandis S.C. 1990. Review of predictive capabilities of JRC-JCS model in engineering practice. *Proc. of Int. Symp. on Rock Joints*, Leon, Norway, Barton & Stephansson, eds., 603-610.

Birch J.S. 2006. Using 3DM Analyst mine mapping suite for rock face characterization. In F.Tonon & J.Kottenstette (eds.), *Laser and Photogrammetric Methods for Rock Face Characterization. Proc. 41st US. Rock Mechanics Symposium,* Golden.

Dawson R.F. 1990. Design guidelines for bedded footwall slopes. MSc. Thesis, University of Alberta, 191 p.

Fardin N., Stephansson O. & Jing L. 2001. The scale dependence of rock joint surface roughness. *Int. J. of Rock Mech. and Min. Sci.*, **38**: 659-669.

Goodman 1989. Introduction to Rock Mechanics, 2nd Edition. John Wiley & Sons, New York.

Grasselli G., Wirth J. & Egger P. 2002. Quantitative three-dimensional description of a rough surface and parameter evolution with shearing. *Int. J. of Rock Mech. and Min. Sci.*, **39**:789-800.

Hebil K. 2006. Pers. comm..

Hoek E. 2007. Practical Rock Engineering. http://www.rocscience.com/hoek/PracticalRockEngineering.asp

Hong E.S., Lee I.M. & Lee J.S. 2006. Measurement of rock joint roughness by 3D scanner. *Geotechnical Testing J.*, **29**: 1-8.

Kulatilake P.H.S.W. & Um J. 1999. Requirements for accurate quantification of self-affine roughness using the roughness-length method. *Int. J. of Rock Mech. and Min. Sci.*, **36**:5-18.

Kulatilake P.H.S.W., Balasingam P., Park J. & Morgan R. 2006. Natural rock joint roughness quantification through fractal techniques. *Geotechnical and Geological Eng.*, **24**:1181-1202.

Kulatilake P.H.S.W., Um J. & Pan G. 1997. Requirements for accurate estimation of fractal parameters for self-affine roughness profiles using the line scaling method. *Rock Mech. Rock Engng.*, **30**:181-206.

Kulatilake P.H.S.W., Um J. & Pan G. 1998. Requirements for accurate quantification of self-affine roughness using the variogram method. *Int. J. Solids Structures*, **35**: 4167-4189.

Rengers N. 1970. Influence of surface roughness on the friction properties of rock planes. *Proc. 2nd Cong. ISRM*, Belgrade, Vol. 1, p. 229-234.

Schneider H.J. 1976. Comment in *Proc. Int. Symp. on Numerical Methods in Soil Mechanics and Rock Mechanics*, G. Borm and H. Meissner, Eds., p. 220-223

Tannant D.D & LeBreton R. 2007. Footwall slope slab failure at a mountain coal mine. *Proc. 1st Canada-US Rock Mech. Symp.*, Vancouver, p.1263-1270.

Tse R. & Cruden D.M. 1979. Estimating joint roughness coefficients. *Int. J. Rock Mech. Min. Sci. & Geomech. Abstr.,* **16**: 303-307.

Yang Z.Y., Lo S.C. & Di C.C. 2001. Reassessing the joint roughness coefficient (JRC) estimation using Z_2. *Rock Mech. Rock Engng.,* **34**: 243-251.

Yu X. & Vayssade B. 1991. Joint profiles and their roughness parameters. *Int. J. Rock Mech. Min. Sci. & Geomech. Abstr.*, **28**: 333-336.